nature immunology

Confinement-optimized three-dimensional T cell amoeboid motility is modulated via myosin IIA–regulated adhesions

Jordan Jacobelli[1], Rachel S Friedman[1], Mary Anne Conti[2], Ana-Maria Lennon-Dumenil[3], Matthieu Piel[3], Caitlin M Sorensen[1], Robert S Adelstein[2] & Matthew F Krummel[1]

During trafficking through tissues, T cells fine-tune their motility to balance the extent and duration of cell-surface contacts versus the need to traverse an entire organ. Here we show that *in vivo*, myosin IIA–deficient T cells had a triad of defects, including overadherence to high-endothelial venules, less interstitial migration and inefficient completion of recirculation through lymph nodes. Spatiotemporal analysis of three-dimensional motility in microchannels showed that the degree of confinement and myosin IIA function, rather than integrin adhesion (as proposed by the haptokinetic model), optimized motility rate. This motility occurred via a myosin IIA–dependent rapid 'walking' mode with multiple small and simultaneous adhesions to the substrate, which prevented spurious and prolonged adhesions. Adhesion discrimination provided by myosin IIA is thus necessary for the optimization of motility through complex tissues.

To perform their surveillance functions, T lymphocytes traffic from the vasculature to secondary lymphoid organs, where they scan for antigenic peptides on cell surfaces[1,2]. In the confinement of these organs, T cells complete a circuit in search of antigen-presenting cells bearing complexes of peptide and major histocompatibility complex. This task is presumed to involve the competing need to carefully survey every surface while also avoiding excessive adhesion that leads to lower motility. The complex choreography of T cell migration has been observed by two-photon microscopy[3,4]; however, the molecular factors that coordinate this process are not well understood.

According to the haptokinetic model, in mesenchymal cells, the density of integrin substrate modulates the optimal rate of motility in two-dimensional environments[5,6]. However, it would seem that integrins on their own are not the main determinant of migration for leukocytes *in vivo*, and they have been shown to be largely dispensable for amoeboid migration in dense collagen matrices and *in vivo*[7–9]. As a general rule, protrusion and force generation during motility are mediated mainly by the actomyosin cytoskeleton through actin polymerization and contraction of the actin network by class II myosin[10–12]. However, the fundamental mechanisms of this process and the factors that regulate motility, particularly *in vivo*, are yet to be fully examined.

Amongst the candidates to regulate optimal T cell amoeboid motility in lymphoid tissues, nonmuscle myosin IIA (A003748; also called NMM-IIA) is speculated to have an important role. Myosin IIA is the only class II myosin expressed in mouse T lymphocytes and is regulated during T cell arrest mediated by engagement of the T cell antigen receptor[13]. In three-dimensional collagen matrices, dendritic cells (DCs) fail to squeeze through packed collagen fibers when myosin II motor function is blocked[7]. Myosin IIA has also been shown to have an important role in mediating efficient T cell migration *in vitro* in two-dimensional environments[13,14]. In some model systems, myosin IIA activity is also important in mediating uropodal detachment from highly adhesive surfaces such as substrates coated with the intercellular adhesion molecule ICAM-1 (A002871)[15,16].

T cells can move by two distinct modes of motility in two-dimensional environments depending on the adhesiveness of the substrate and on myosin IIA activity[14]. On low-adhesive two-dimensional surfaces, T cells show fast amoeboid crawling motility that requires myosin IIA–generated contractile forces and uses multiple concurrent surface contacts ('walking'). In contrast, on highly adhesive surfaces, T cell crawling uses a single-surface contact, resembles the migration of fibroblasts and epithelial cells and is driven mainly by actin polymerization ('sliding'). Data also indicate that myosin IIA activity restricts surface adhesion on two-dimensional substrates[14], but the relevance of this finding to motility in lymph nodes and highly confined environments with many possible surface contacts is unclear. The interaction of confinement, provided in three-dimensional environments, and adhesiveness during motility also remains unexplored.

Here we show that myosin IIA function had a role in many steps of T cell trafficking, including interstitial migration of T cells and lymph node retention. Ablation of myosin IIA led to many defects, which

[1]Department of Pathology, University of California San Francisco, San Francisco, California, USA. [2]Laboratory of Molecular Cardiology, National Heart, Lung, and Blood Institute, National Institutes of Health, Bethesda, Maryland, USA. [3]Institut National de la Santé et de la Recherche Médicale U653, Institut Curie, Paris, France. Correspondence should be addressed to M.F.K. (matthew.krummel@ucsf.edu).

Received 24 June; accepted 17 August; published online 12 September 2010; doi:10.1038/ni.1936

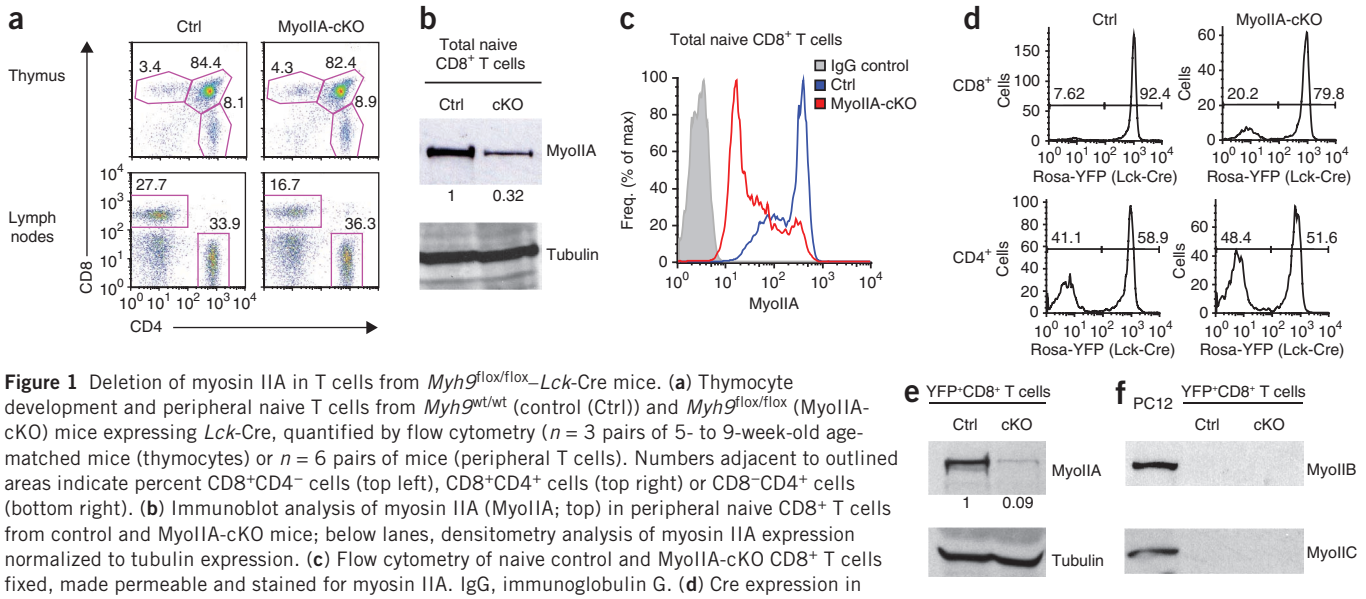

Figure 1 Deletion of myosin IIA in T cells from *Myh9*$^{flox/flox}$–*Lck*-Cre mice. (**a**) Thymocyte development and peripheral naive T cells from *Myh9*$^{wt/wt}$ (control (Ctrl)) and *Myh9*$^{flox/flox}$ (MyoIIA-cKO) mice expressing *Lck*-Cre, quantified by flow cytometry ($n = 3$ pairs of 5- to 9-week-old age-matched mice (thymocytes) or $n = 6$ pairs of mice (peripheral T cells). Numbers adjacent to outlined areas indicate percent CD8$^+$CD4$^-$ cells (top left), CD8$^+$CD4$^+$ cells (top right) or CD8$^-$CD4$^+$ cells (bottom right). (**b**) Immunoblot analysis of myosin IIA (MyoIIA; top) in peripheral naive CD8$^+$ T cells from control and MyoIIA-cKO mice; below lanes, densitometry analysis of myosin IIA expression normalized to tubulin expression. (**c**) Flow cytometry of naive control and MyoIIA-cKO CD8$^+$ T cells fixed, made permeable and stained for myosin IIA. IgG, immunoglobulin G. (**d**) Cre expression in mature single-positive CD8$^+$ and CD4$^+$ T cells in the lymph node, assessed with the Rosa-YFP reporter. (**e**) Immunoblot analysis of myosin IIA in sorted YFP$^+$CD8$^+$ peripheral T cells from *Myh9*$^{wt/wt}$–*Lck*-Cre$^+$ Rosa-YFP mice (Ctrl) and *Myh9*$^{flox/flox}$–*Lck*-Cre$^+$ Rosa-YFP mice (cKO); below, densitometry as in **b**. (**f**) Expression of myosin IIB (MyoIIB) and myosin IIC (MyoIIC) in sorted YFP$^+$-CD8$^+$ *Myh9*$^{wt/wt}$–*Lck*-Cre$^+$ and *Myh9*$^{flox/flox}$–*Lck*-Cre$^+$ Rosa-YFP peripheral T cells; the PC12 rat neuronal-like cell line serves as a positive control. Data are representative of three independent experiments.

broadly suggested a generalized lack of cortical control and promiscuous cell-substrate interactions. Using engineered 'microchannels' designed to provide various amounts of confinement, such as those that may be found in tissues *in vivo*, we found that myosin IIA was a key participant in facilitating rapid motility and the ability to release from one surface contact and move to another. As in two-dimensional environments, myosin IIA allowed cells under confinement to maximize their speed. Notably, the main determinant of the optimal environmental and intracellular conditions required to achieve rapid motility was an ideal degree of confinement coupled with myosin IIA function, and this optimum was less dependent on integrin density than it was in two-dimensional mesenchymal models. Using total internal reflection fluorescence (TIRF) imaging, we found that under these optimum conditions, T cells migrated by a walking mode. This myosin IIA–dependent motility mode permitted T cells to make selective contacts with the substrate, minimizing their effective drag and allowing rapid movements between surfaces and in complex and dense environments.

RESULTS

T cells from mice with conditional knockout of myosin IIA

T lymphocytes alternate between walking and sliding modes of motility based in part on myosin IIA activity[14], and we sought to determine how these mechanisms function in interstitial environments. Myosin IIA is the only class II myosin expressed in mouse T cells[13], and germline knockout of the gene encoding myosin IIA results in embryonic death[17]. To eliminate myosin IIA specifically from naive T cells, we used a Cre recombinase–mediated conditional knockout strategy targeting the gene encoding the myosin IIA heavy chain (*Myh9*; **Supplementary Fig. 1**). We deleted myosin IIA expression during the single-positive stage of thymocyte development by crossing mice with *lox*P-flanked *Myh9* alleles (*Myh9*$^{flox/flox}$) with a transgenic mouse line expressing Cre recombinase under the control of a modified distal promoter of the gene encoding the kinase *Lck* (*Lck*-Cre)[18]. As controls for our experiments, we used either *Myh9*$^{wt/wt}$–*Lck*-Cre$^+$ mice or *Myh9*$^{flox/flox}$–*Lck*-Cre$^-$ mice and obtained similar results with each. The *Myh9*$^{flox/flox}$–*Lck*-Cre$^+$ (MyoIIA-cKO) mice had normal percentages of single-positive CD4$^+$ and CD8$^+$ thymocytes (**Fig. 1a**). Mature T cells were present in the periphery, although MyoIIA-cKO mice had fewer CD8$^+$ T cells than did control (*Myh9*$^{wt/wt}$–*Lck*-Cre$^+$) mice (**Fig. 1a**). On average, the frequency of CD8$^+$ T cells in lymph nodes was 22.1% for control mice and 13.9% for MyoIIA-cKO mice, and 13.9% and 7.0%, respectively, in the blood. The lower numbers were probably due to shorter long-term survival of the myosin IIA–deficient CD8$^+$ T cells in the periphery rather than a thymic exit defect, given the normal thymic populations. Furthermore, when we compared the ratio of the percentage of CD8$^+$ T cells in the lymph nodes of MyoIIA-cKO mice to that of CD8$^+$ T cells in the lymph nodes of control mice (63% of control) with the ratio of the percentages in the blood (50% of control), this suggested a trend toward accumulation of CD8$^+$ T cells in the lymph nodes of MyoIIA-cKO mice.

The total pool of naive CD8$^+$ MyoIIA-cKO T cells expressed one third the myosin IIA protein detected in control cells (**Fig. 1b**). This was apparently the result of partial Cre expression in this population, as on average, ~85% of MyoIIA-cKO CD8$^+$ T cells had much lower expression of myosin IIA protein, but a subpopulation of ~15% of CD8$^+$ T cells had myosin IIA expression similar to that of control cells (**Fig. 1c**). To confirm the efficacy of our conditional knockout approach and the penetrance of Cre expression in T cell populations, we crossed control and MyoIIA-cKO mice with transgenic mice containing a knock-in of yellow fluorescence protein (YFP) in the Gt(Rosa)26Sor locus[19] (Rosa-YFP mice). In these mice, YFP expression is dependent on Cre expression as a result of an upstream stop codon cassette flanked by *lox*P sites. We determined that in control (*Myh9*$^{wt/wt}$–*Lck*-Cre$^+$) and MyoIIA-cKO Rosa-YFP mice, Cre expression was present in 80–95% of CD8$^+$ T cells but in only 50–60% of CD4$^+$ T cells (**Fig. 1d**). Immunoblot analysis of sorted Rosa-YFP$^+$ CD8$^+$ T cells from control and MyoIIA-cKO mice routinely demonstrated that Cre$^+$ CD8$^+$ T cells from MyoIIA-cKO mice had ~90% lower myosin IIA protein expression (**Fig. 1e**). This confirmed efficient deletion of myosin IIA in Cre-expressing *Myh9*$^{flox/flox}$ cells. It is possible that after myosin IIA deletion, other class II isoforms could be upregulated in T cells. However, we did not detect expression of

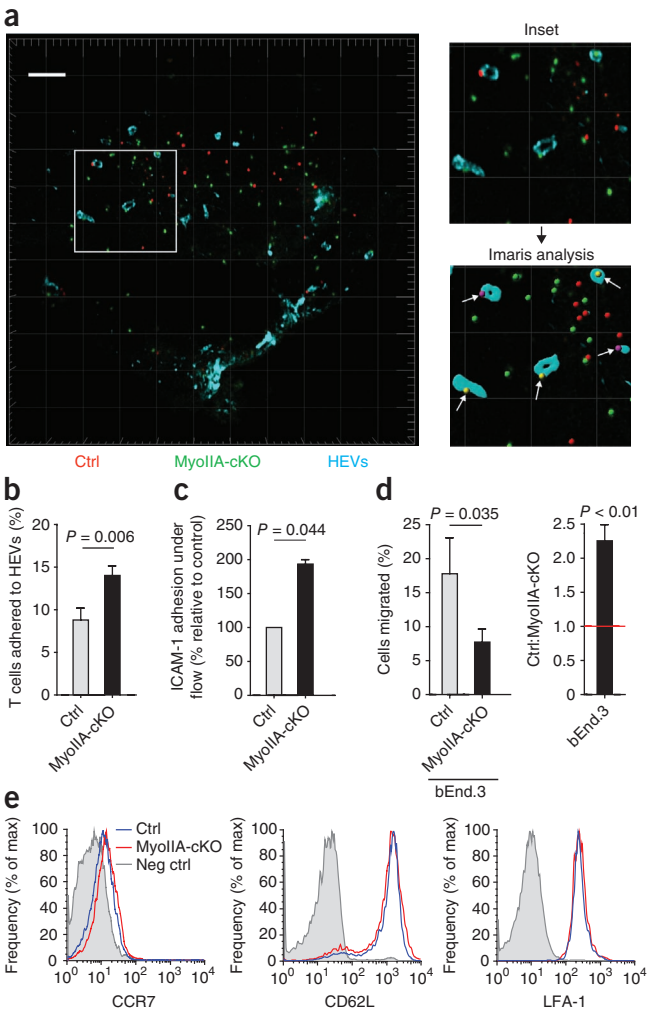

Figure 2 MyoIIA-cKO T cells have more contact with HEVs and adhesion to integrin substrates. (**a**) Cryosection of a popliteal lymph node collected 2 h after adoptive cotransfer of a 1:1 mixture of fluorescence-labeled naive control CD8$^+$ T cells (red) and naive MyoIIA-cKO CD8$^+$ T cells (green); sections were stained with antibody to peripheral node addressin-1 for visualization of HEVs (blue). Top right, higher magnification of boxed area at left, showing T cells in contact with HEVs; bottom right, HEV surface rendering with Imaris software from the image above, showing identification of cells in contact with HEVs (arrows). Scale bar and light gray grid intervals, 100 μm. (**b**) Frequency of control and MyoIIA-cKO T cells in contact with HEVs 2 h after transfer as in **a** ($n = 4$ lymph node sections per experiment with ~50 cells per group per lymph node section). (**c**) Adherence of control and MyoIIA-cKO CD8$^+$ T cells after injection into flow chambers and 10 min of physiological shear flow (2 dyne/cm^2). (**d**) Frequency of transendothelial migration (left) of control and MyoIIA-cKO T cells through a bEnd.3 endothelial cell monolayer seeded on Transwells (5-μm pore) in response to CCL21 (1 μg/ml). Right, ratio of transmigrated control T cells to transmigrated MyoIIA-cKO T cells. (**e**) Expression of CCR7, CD62L and LFA-1 by naive CD8$^+$ T cells from control and MyoIIA-cKO mice. Data are representative of three independent experiments (**a**,**e**) or are from three independent experiments (**b**–**d**; average and s.e.m.).

myosin IIB or myosin IIC protein in sorted Rosa-YFP$^+$ CD8$^+$ T cells from control or MyoIIA-cKO mice (**Fig. 1f**). On the basis of our results for Cre penetrance in CD4$^+$ versus CD8$^+$ T cell subsets, we focused our work on the motility of CD8$^+$ T cells. To avoid subjecting naive T cells to cell sorting, and given that on average 85% of CD8$^+$ T cells from MyoIIA-cKO mice had efficient depletion of myosin IIA, we used total CD8$^+$ T cells for our subsequent experiments.

Myosin IIA regulates adhesion under flow

Analysis of differently labeled transferred myosin IIA–deficient and control T cells did not show a gross alteration of their overall localization in lymph node T cell zones 2 h after transfer. However, loss of myosin IIA resulted in a ~60% greater frequency of contact of MyoIIA-cKO naive T cells with high-endothelial venules (HEVs) at this time point (**Fig. 2a**,**b**). Rolling and firm adhesion are critical steps in T cell extravasation, and a possible reason for the observed accumulation of MyoIIA-cKO cells at HEVs could have been more adhesion, particularly under flow. Therefore, we measured the ability of myosin IIA–deficient T cells to adhere and remain attached to ICAM-1-coated surfaces in the presence of chemokine under physiological shear flow. Naive MyoIIA-cKO T cells had twofold greater adhesion to ICAM-1 under flow (**Fig. 2c**), which confirmed our finding of overadhesion *in vivo*. However, when we next measured the ability of myosin IIA–deficient naive T cells to transmigrate through endothelial cell monolayers plated on Transwell membranes, MyoIIA-cKO naive T cells had ~50% less migration across endothelial cells than did control naive T cells (**Fig. 2d**). To rule out the possibility that the greater adhesion of myosin IIA–deficient T cells *in vitro* and *in vivo* was due to altered surface expression of chemokine or adhesion receptors, we verified that naive control and myosin IIA–deficient CD8$^+$ T cells had similar expression of the chemokine receptor CCR7, the lymph node–homing receptor L-selectin (A001417; CD62L) and the integrin $\alpha_L\beta_2$ (LFA-1; **Fig. 2e**).

Myosin IIA controls interstitial T cell motility *in vivo*

To address how modulation of actomyosin dynamics by myosin IIA affected T cell interstitial migration in the lymph nodes, we used two-photon microscopy analysis of adoptively transferred naive control and MyoIIA-cKO CD8$^+$ T cells. MyoIIA-cKO T cells had much shorter track lengths and less displacement from their origin (**Fig. 3a**,**b** and **Supplementary Movie 1**). Myosin IIA–deficient cells showed a 26% average lower median speed and a lower frequency of cells that reached peak instantaneous velocities (**Fig. 3c**). The median turning angle between time points of MyoIIA-cKO T cells was also increased from 47.5° to 54° per turn (**Fig. 3d**). Although these defects were numerically modest, they compounded over time and resulted in an average decrease of 45% in the mean square displacement of myosin IIA–deficient T cells over a 10-minute time period (**Fig. 3e**). Furthermore, the average motility coefficient, used as a measure of the volume a cell can survey over time[20], was decreased by 49% ($P = 0.009$) over a 10-minute time period in MyoIIA-cKO T cells, from 27.7 μm/√min to 14.2 μm/√min. MyoIIA-cKO T cells also had a greater frequency of arrested cells (26.8% versus 11.6%; $P = 0.0118$), defined as cells that do not move more than 10 μm from their origin during an interval of 5 min or more.

The greater confinement of MyoIIA-cKO T cells could be attributed to an inability to sense and follow a directional chemotactic cue. To assess this, we measured both chemotactic migration (response to a directional gradient of chemokine) and chemokinetic migration (response to the presence of chemokine) of naive control and myosin IIA–deficient CD8$^+$ T cells across 5-μm pore Transwells. MyoIIA-cKO T cells showed 64% less chemotaxis toward the chemokine CCL21 than did control cells (**Fig. 3f**). However, chemokinesis was inhibited to the same extent, which suggested that the migration defects were not due exclusively to impaired chemotaxis of myosin IIA–deficient T cells.

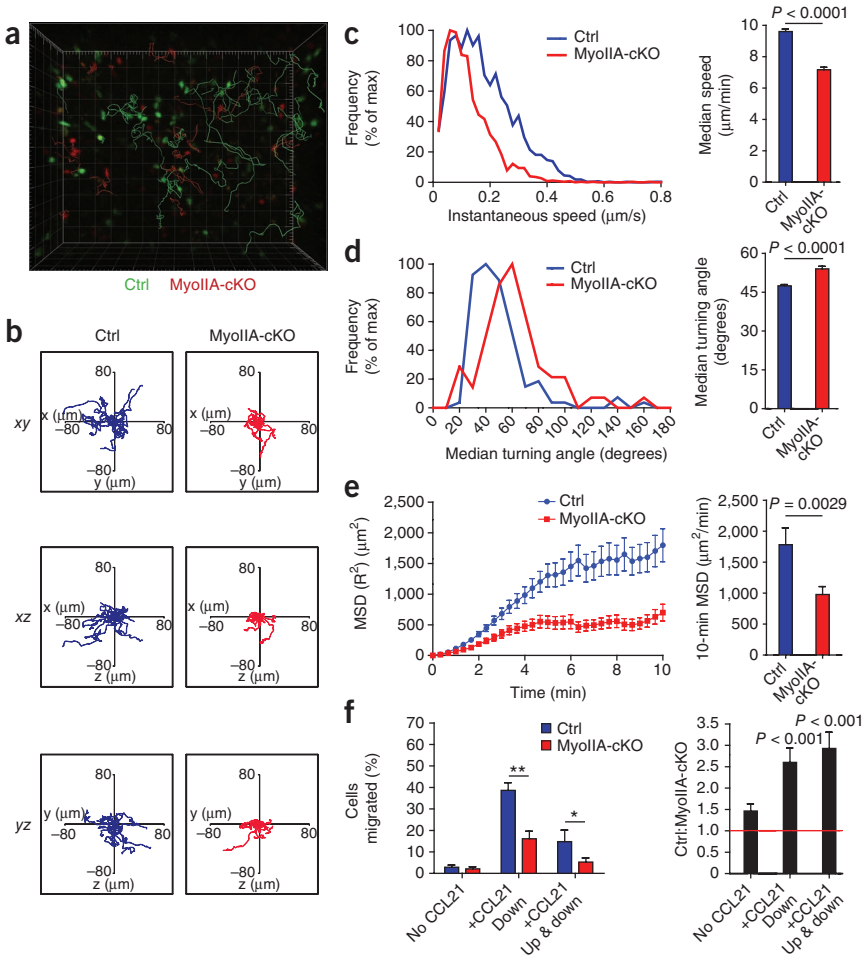

Figure 3 Naive myosin IIA–deficient T cells have less intra–lymph node migration. Time-lapse two-photon microscopy of lymph nodes from recipients of intravenous injection of labeled naive control and MyoIIA-cKO CD8$^+$ T cells. (**a**) Three-dimensional reconstruction of a stage position with tracks overlaid: green, control cells; red, MyoIIA-cKO cells (20 randomly selected tracks). Grid marks, 20 μm. (**b**) Tracks of control and MyoIIA-cKO T cells over a time span of 10 min (15 randomly selected tracks). (**c**) Distribution of instantaneous velocities (left) and average median velocity (right) of control and MyoIIA-cKO T cells. (**d**) Distribution of mean turning angles (left) and average median turning angle (right) of control and MyoIIA-cKO T cells. (**e**) Mean square displacement (MSD) over time (left) and average mean square displacement over 10 min (right) of control and MyoIIA-cKO T cells. (**f**) Frequency of migration of control and MyoIIA-cKO naive T cells in response to no CCL21 (left) or to CCL21 (1 μg/ml) added to the bottom well (middle; chemotaxis) or to both the top and bottom chambers (right; chemokinesis) of a Transwell. *$P < 0.01$ and **$P < 0.001$. Right, ratio of transmigrated control T cells to transmigrated MyoIIA-cKO T cells. Data are from one stage position representative of three independent experiments (**a**,**b**, and **c**–**e**, left), are averaged from three independent experiments (**f**) or are pooled from multiple lymph nodes from each of three independent experiments (**c**–**e**, right; error bars, s.e.m. in **c**–**f**).

Myosin IIA regulates the lymph node recirculation of naive T cells

The transmigration and interstitial motility defects of myosin IIA–deficient T cells prompted us to characterize the role of this myosin in the trafficking and recirculation of naive T cells. After adoptive transfer, we observed more myosin IIA–deficient naive CD8$^+$ T cells than control naive CD8$^+$ T cells in lymph nodes (**Fig. 4a**). This accumulation increased over time between 2 h and 42 h after transfer, to a maximum of 1.9-fold (**Fig. 4b**). This could potentially have been caused by more entry into and/or less egress from lymph nodes. Our data on *in vitro* transendothelial migration of MyoIIA-cKO T cells indicated that greater entry was unlikely. To determine whether impaired exit from lymph nodes had a role in this accumulation, we adoptively transferred control and MyoIIA-cKO T cells into recipient mice and allowed them to equilibrate for 24 h, then blocked further T cell entry into lymph nodes through the use of blocking antibody to CD62L (anti-CD62L). There were 3.3-fold more naive myosin IIA–deficient T cells than naive control T cells in mice treated with anti-CD62L, compared with 1.8-fold in the absence of entry blockade (**Fig. 4c**). This indicated that myosin IIA has a role in the rate at which T cells exit lymph nodes. Given the greater adhesion of MyoIIA-cKO T cells to ICAM-1 and on HEVs, we also used LFA-1- and integrin α_4–blocking antibodies to rule out the possibility that MyoIIA-cKO T cells could be entering lymph nodes even after CD62L blockade. The 3.2-fold greater number of myosin IIA–deficient T cells relative to that of control cells under this blockade confirmed that the accumulation of MyoIIA-cKO cells was due largely to lymph node retention (**Fig. 4d**).

Myosin IIA–deficient T cells did not show significantly more accumulation at the surface of lymphatic sinuses (**Fig. 4e**,**f**), which suggested that less exit from lymph nodes was probably due to more interstitial confinement of myosin IIA–deficient T cells rather than to deficiencies in passage through the sinuses.

Optimal confinement and myosin IIA maximize motility

Given the three-dimensional organization of the lymph node and that directional chemotaxis of MyoIIA-cKO T cells was not completely abrogated, we hypothesized that the myosin IIA–dependent migration defects could be caused by overadherence to surrounding surfaces in confined environments. Therefore, we sought a method to delineate the role of cellular adhesion and contractility during migration in three-dimensional environments as a contributor to the *in vivo* migration defects of MyoIIA-cKO T cells. For this we used microfabricated channels (microchannels)[21] of various sizes to provide a platform in which T cells could be variably confined in two dimensions while allowing motility in the third dimension (**Fig. 5a**). We created these channels with a constant ceiling height and with variable width to either confine the cells or allow them to meander to different degrees from side wall to side wall (**Fig. 5b** and **Supplementary Movie 2**). Microchannels can be assembled on glass coverslips, allowing imaging of the details of the adhesive contacts (by TIRF microscopy) on one surface during migration and extrapolation of the nature of these contacts to the other dimensions. We used activated T cells for most of these experiments, as they had myosin IIA–dependent defects similar to those of naive T cells when analyzed both *in vivo* (**Supplementary Fig. 2**) and during transmigration *in vitro* (data not shown).

First we analyzed whether the degree of confinement affected T cell motility. For these experiments we used microchannels with

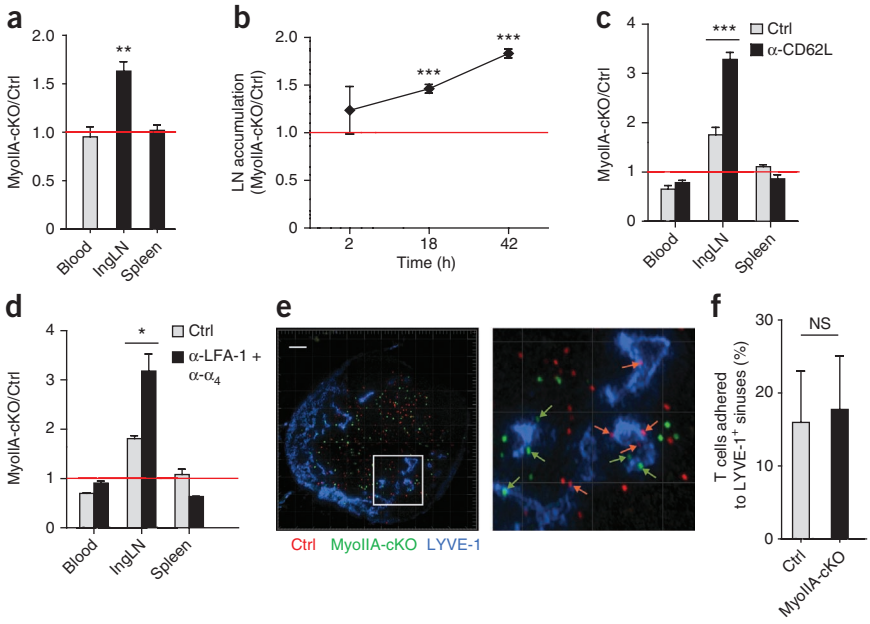

Figure 4 Naive myosin IIA–deficient T cells have trafficking defects *in vivo* due to retention in the lymph nodes. (**a**) MyoIIA-cKO and control T cells in the blood, inguinal lymph nodes (IngLN) and spleens of recipient mice 18–42 h after transfer, quantified by flow cytometry as the ratio of MyoIIA-cKO to control; ratios for lymph node and spleen are presented relative to those for blood. (**b**) Time course of the accumulation of MyoIIA-cKO T cells in the inguinal lymph nodes of recipient mice at 2, 18 and 42 h after transfer, quantified as in **a** and presented relative to the ratio in blood. (**c**) Control and MyoIIA-cKO T cells in the blood, inguinal lymph nodes and spleen 18 h after treatment with PBS or anti-CD62L (α-CD62L), presented as the ratio of MyoIIA-cKO cells to control cells relative to the ratio in blood, as in **a**. (**d**) Control and MyoIIA-cKO T cells in the blood, inguinal lymph nodes and spleen 18 h after treatment with PBS or integrin-blocking antibodies, presented as in **c**. (**e**) Cryosection of a popliteal lymph node 42 h after adoptive transfer of labeled control T cells (red) and MyoIIA-cKO T cells (green), stained with antibody to the lymphatic endothelial cell marker LYVE-1 for visualization of lymphatic endothelium (blue). Right, higher magnification of boxed area at left containing T cells in contact with the lymphatic endothelium (red and green arrows). Scale bar and light gray grid intervals, 100 μm. (**f**) Frequency of control and MyoIIA-cKO T cells in contact with lymphatic endothelium 42 h after adoptive transfer. Multiple lymph node sections were analyzed with an average of 50 cells for each group per lymph node section. $*P < 0.05$, $**P < 0.01$ and $***P < 0.001$. Data are from at least four independent experiments (**a**–**c**) or two (**d**) or three (**e**,**f**) independent experiments (average and s.e.m.).

a fixed ceiling height of 7 μm, a dimension similar to the girth of an activated T cell. We also determined how differences in the adhesiveness of the substrate may influence confined T cell migration by coating the microchannels with fibronectin, ICAM-1 or casein (which is not an integrin ligand and blocks the binding of integrin ligands to the substrate; **Fig. 5c**–**e**). In all cases, we observed peak velocity at optimal confinement and lower speed for cells too tightly or too loosely enclosed. In microchannels with widths that approximated their girth (7–9 μm), T cells migrated at a peak average velocity that exceeded 20 μm/min in the presence of the integrin substrates fibronectin and ICAM-1 (**Fig. 5c**,**d**). T cell speed was lower at smaller microchannel widths (4–5 μm), probably because of more cell surface friction along the channel walls. The other extreme of less confinement (12- to 20-μm microchannels) was also nonoptimal, as we observed lower speed, possibly due to suboptimal availability of surfaces to push off and adhere to or to inefficiencies associated with protrusions in directions orthogonal to the direction of propagation. Notably, although T cells migrating in casein-coated microchannels did not achieve the same average speeds detected in fibronectin- and ICAM-1-coated microchannels, we still observed a similar confinement-dependent distribution of migration velocities in control cells (**Fig. 5e**). This suggested that confinement is a chief determinant of motility speed and only to a lesser extent is the presence of integrin substrate necessary to achieve this optimum.

To characterize the role of myosin IIA in migration in microchannels, we used the class II myosin chemical inhibitor blebbistatin[22] and imaging conditions that avoid photoinactivation and toxicity of this drug. The use of blebbistatin gave us the ability to acutely and completely inhibit the function of myosin IIA, complementing the MyoIIA-cKO approach. Under these conditions, inhibition of myosin IIA resulted in an overall lower motility of activated T cells across all microchannel sizes, with average speeds that did not change much relative to the confinement (**Fig. 5c**–**e**). In particular, under conditions in which control cells achieved maximal motility (7- to 8-μm microchannels), T cells with inhibited myosin IIA did not have an average speed much greater than their speed in microchannels with more or less confinement. This suggested that myosin IIA function is required not only for fast motility in general but specifically for T cells to adapt their motility mode to the environment. Furthermore, as we observed similar motility rates when myosin IIA was blocked in the casein- and integrin-substrate coated conditions, we conclude that the function of myosin IIA in optimizing motility is not strictly dependent on the binding of integrin to the substrate.

Further analysis of T cell motility in larger microchannels (greater than a cell width) coated with fibronectin provided additional evidence to support the idea of complex interaction of surface contacts. In this setting, activated T cells constantly switched adherence (weaved) between opposing walls of the microchannel rather than crawling forward along one of the channel walls (**Fig. 6a** and **Supplementary Movie 3**). Such weaving could result from a T cell analog of the 70° average bifurcation in the protrusions generated during motility in *Dictyostelium*[23]. T cells with inhibited myosin IIA became more adherent to the channel walls between weaves, which resulted in a much lower weaving frequency (**Fig. 6a** and **Supplementary Movie 4**). Blebbistatin-treated T cells had a doubling of the time that elapsed from initial adhesion to one side wall of the channel to contact with the other (weaving cycle; **Fig. 6b**). This was not a function of the lower velocity of myosin IIA cells in the presence of blebbistatin, as shown by the finding that the adhesion time to a channel wall of T cells with inhibited myosin IIA was also doubled (**Fig. 6b**). In sum, these experiments indicate that myosin IIA functions to limit adhesion to the substrate for confinement-optimized motility.

To specifically analyze the nature of the coupling of cells to surfaces under three-dimensional confinement, we used TIRF microscopy of T cells in microchannels to visualize the adhesive contacts

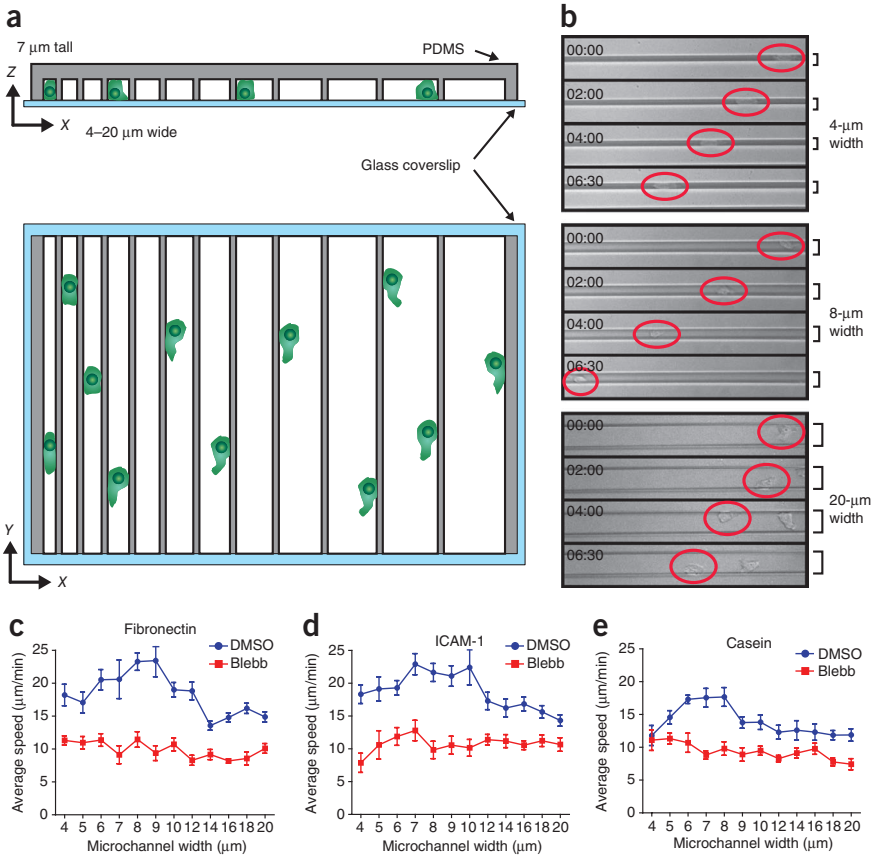

Figure 5 T cell migration efficiency in confined environments is controlled by myosin IIA. (**a**) Variable microchannel array assembly. PDMS, polydimethylsiloxane. (**b**) Brightfield time-lapse microscopy of vehicle-treated CD8$^+$ T cells 4–5 d after activation, injected into microfabricated confining channels of various sizes (right margin) in the presence of vehicle control or 100 μM blebbistatin. Red circles outline T cell positions; numbers in top right corners indicate time (in min:s). (**c**–**e**) Speed of dimethyl sulfoxide (DMSO)- or blebbistatin (Blebb)-treated activated CD8$^+$ T cells injected into microchannels coated with fibronectin (**c**), ICAM-1 (**d**) or casein (**e**), presented as a function of microchannel width. Data are representative of three (**b**,**c**) or two (**d**,**e**) independent experiments (mean ± s.e.m. of ten or more cells per microchannel width per treatment condition in **c**–**e**).

on the surface nearest the objective. Loss of myosin IIA results in a shift in the crawling mode of CD4$^+$ T cell clones during two-dimensional migration, which is associated with more adherence[14]. TIRF imaging of activated control T cells in microchannels indicated that these cells migrated mainly by amoeboid crawling with multiple small independent surface contact points (walking; **Fig. 6c**,**d** and **Supplementary Movie 5**). Thus, although cells seemed elongated, they were effectively 'choosing' only specific points of the membrane for surface contact, thereby potentially limiting frictional drag while permitting dynamic scanning of new areas. Blebbistatin-induced loss of myosin IIA activity resulted in a change in motility mode, with T cells mainly crawling using one large adhesion area (sliding) and with prolonged contacts on a given microchannel wall (**Fig. 6c**,**d** and **Supplementary Movie 6**). Although cells using this mode are still able to crawl forward, this mode results in more drag surface that involves a greater portion of the cell cortex and probably slows the cell.

Finally, although it was technically challenging because of their lower motility and entry into microchannels, we also analyzed the migration of naive T cells in microchannels (with a ceiling height of 3 μm because of their smaller size). Generally, naive T cells were less motile than activated T cells, particularly under less confinement (channels >10 μm; **Supplementary Fig. 3**); this also confirmed that larger channels do not support optimal motility rates. Nonetheless, comparison of the migration of control and MyoIIA-cKO naive T cells in microchannels with a width of 4 μm or 8 μm supported the idea of a role for myosin IIA as a determinant in optimizing T cell motility in confinement (**Supplementary Fig. 3**).

Overadhesion of myosin IIA–deficient T cells

TIRF microscopy showed that blebbistatin-treated activated CD8$^+$ T cells had a significantly greater adhesion area than did vehicle-treated activated CD8$^+$ T cells when plated on casein- or ICAM-1-coated surfaces (**Fig. 7a**,**b**). This was also true for MyoIIA-cKO naive CD8$^+$ T cells compared with control naive CD8$^+$ T cells plated on ICAM-1 (**Fig. 7c**). The adhesion area of naive T cells plated on casein coated surfaces was too small to be consistently detected by our TIRF imaging method. Furthermore, similar to published observations[13], inhibition of myosin IIA also resulted in an altered cell morphology, with more rounding of activated T cells, as shown by measurement of their shape factor (which indicates how circular a cell is) and ellipticity (cell length/cell breadth; **Supplementary Fig. 4**). Overall, these data are consistent with the idea of a role for myosin IIA in modulating T cell surface contacts in both the presence and absence of integrin ligands.

In vivo in the lymph node paracortex, T cells are believed to follow tracks defined by a dense network of fibroblastic reticular cells (FRCs)[24], and it has been shown that FRCs can provide chemokines to support the adhesion and migration of T cells[25,26]. Therefore, we tested whether overadhesion of T cells in the absence of myosin IIA function resulted in more contact with FRCs and caused the slower and more meandering motility of MyoIIA-cKO T cells *in vivo*. To determine the extent of adhesion of T cells to FRCs *in vivo*, we generated bone marrow chimeras by reconstituting irradiated mice expressing cyan fluorescent protein (CFP) under control of the actin promoter (actin-CFP mice) with bone marrow cells from wild-type mice[24]. Imaging of labeled control and MyoIIA-cKO naive T cells transferred into the chimeric mice did not show a significant difference in the percentage of MyoIIA-cKO naive T cells or control cells that potentially interacted with FRCs in lymph nodes (**Fig. 7d**).

We therefore considered other cells present in lymph nodes as candidates for adhesion and frictional drag. We quantified the adhesion of T cells to other lymph node–dwelling cells, such as lymphatic endothelial cells, DCs and other T cells. Our *in vitro* coupling data confirmed that myosin IIA–deficient naive T cells did not interact more with FRCs and showed that their percentage of attachment to

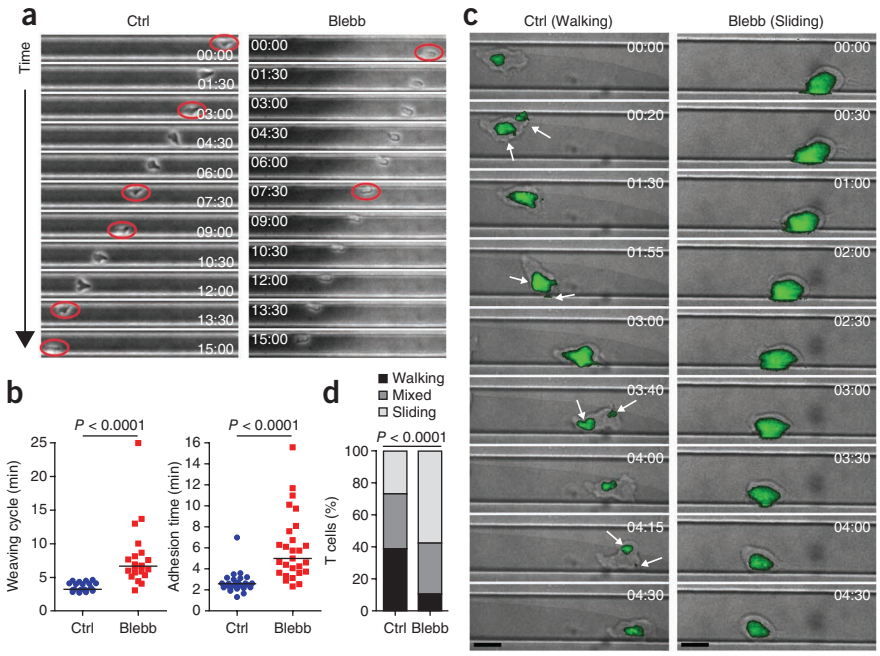

Figure 6 Myosin IIA regulates the crawling mode of T cells under confinement. (**a**) Weaving of CD8$^+$ T cells injected into fibronectin-coated microchannels 20 μm in width 4–5 d after activation in the presence of vehicle control (left; Ctrl) or 100 μM blebbistatin (Blebb; right), presented over time (top right corners, in min:s) at intervals of 1.5 min. Red circles indicate the initial time at which a cell switched between microchannel walls. (**b**) Time interval of 'weaving' between walls (left) and median duration of contact with a microchannel wall (right) for control and blebbistatin-treated cells in fibronectin-coated microchannels 18–20 μm in width. Each symbol represents an individual cell; small horizontal lines indicate the median. (**c**) Brightfield images of a walking control T cell (left) and a sliding blebbistatin-treated cell (right) migrating over time in fibronectin-coated microchannels 18 μm in width, overlaid with TIRF adhesion area images (green); images were obtained at intervals of 5 s for 5 min. Labeling of T cells with the cell-tracking dye CMTMR allowed TIRF 'readout' of adhesion areas without illumination of cells at wavelengths below 500 nm. White arrows (left) indicate multiple distinct adhesion zones. Scale bars, 10 μm. (**d**) Frequency of crawling modes of control and blebbistatin-treated cells in microchannels 10 μm in width ($n > 82$ cells per treatment group). Data are representative of or are pooled from three (**a**,**b**) or two (**c**,**d**) independent experiments.

lymphatic endothelial cells and DCs was also similar to that of control naive T cells (**Fig. 7e**). However, MyoIIA-cKO T cells had ~60% more attachment to other T cells than did control cells (**Fig. 7e**). In the T cell zones of lymph nodes, T cells are probably constantly in proximity with other surrounding lymphocytes, and these prolonged interactions would be predicted to cause excessive drag, resulting in less motility and more meandering *in vivo*.

DISCUSSION

Lymphocyte migration *in vivo* relies on coordinated regulation of actin polymerization and branching, as suggested by work with T cells deficient in upstream regulators of the actin-nucleator protein Arp2/3, such as WASP[27], Dock2 (ref. 28) and coronin-1A[29,30]. However, the role of class II myosin during interstitial T cell migration has remained unknown. Our work here has indicated a requirement for myosin IIA function in lymphocyte migration and trafficking *in vivo*. Notably, we have provided new insight into the extent and dynamics of surface contacts as important factors regulating three-dimensional lymphocyte migration.

Microfabricated channels allowed us to recapitulate some aspects of the environmental confinement that lymphocytes may encounter *in vivo* and permitted us to demonstrate the existence of a confinement optimum for amoeboid motility. The presence of integrin ligands had only a limited effect on this optimization, in contrast to what would be

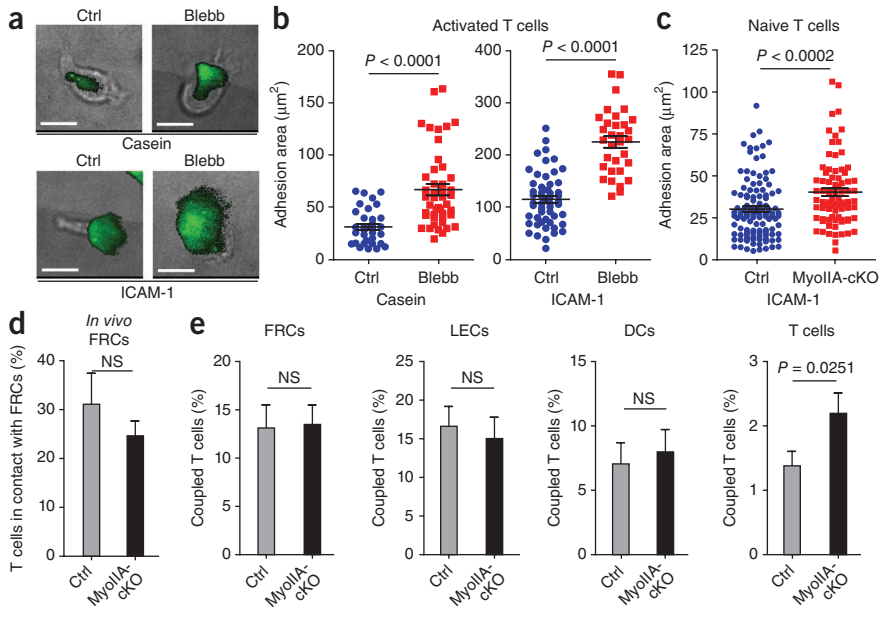

Figure 7 Deregulated surface adhesion of T cells lacking myosin IIA. (**a**) Adhesion areas of control and blebbistatin-treated activated CD8$^+$ T cells plated on glass coated with casein or ICAM-1, assessed by TIRF microscopy (green) and brightfield microscopy. Scale bars, 10 μm. (**b**) Quantification of the adhesion areas of control and blebbistatin-treated activated CD8$^+$ T cells on casein (left) or ICAM-1 (right). (**c**) Quantification of the adhesion areas of naive control and MyoIIA-cKO CD8$^+$ T cells plated on ICAM-1. Each symbol represents an individual cell; small horizontal lines indicate mean ± s.e.m. (**b**,**c**). (**d**) Frequency of transferred control and MyoIIA-cKO naive T cells in contact with the FRC network in actin-CFP chimeric mice, quantified by two-photon microscopy. (**e**) Conjugation frequency (average) of cytosolic dye CFSE–labeled naive control or MyoIIA-cKO CD8$^+$ T cells with CMTMR-labeled FRCs, lymphatic endothelial cells (LECs), DCs or naive T cells, quantified by flow cytometry after 10 min of incubation together. Data are representative of or pooled from at least two independent experiments (**a**–**c**) or are pooled from at least three independent experiments (**d**,**e** (multiple stage positions in **d**); error bars, s.e.m.).

predicted from the haptokinetic model and in agreement with studies of leukocyte migration *in vivo*[7,8]. Indeed, faced with low-adhesive substrates, amoeboid cells can adapt by increasing actin-polymerization rates during protrusion to compensate for less force-coupling[31]. This is also consistent with the idea of 'chimneying' described for cells crawling between adjacent coverslips[32].

Under ideal confinement, we observed migration speeds of over 20 μm/min; these were greater than average speeds but equivalent to the highest instantaneous speeds reported for motility in lymph nodes. This could have been due to the fact that individual microchannels provide a consistent and in some cases optimized environment (~8-μm channels) for T cell migration. In contrast, in lymph nodes, lymphocytes probably encounter various microenvironments with different characteristics, which may modulate motility speeds and limit peak velocities. Furthermore, in the absence of myosin IIA function, T cells did not achieve optimal motility in microchannels, probably because of hyperadhesion and spreading, which cause more friction and drag. In this context, regulation of cortical tension and adhesion by myosin IIA can modulate the ability of lymphocytes to adapt their morphology to optimize their interaction with the environment during motility.

We propose that the motility optimum is reached at amounts of confinement at which three things coincide. First, the ability to contact and exert force on multiple adjacent surfaces is maximized, which optimizes frictional coupling without the need for highly specific protein-protein interactions. Second, inefficiencies from actin-based protrusion along incorrect axes are minimized. Third, the cell can restrict the extent of cortical contact with the substrate, minimizing excessive drag. Under extreme confinement, the size and rigidity of the nucleus may limit how thin the cell can become, forcing the cortex to drag along even when not in use for force coupling. It has been proposed that myosin IIA might overcome such nucleus-induced drag when dendritic cells migrate through dense collagen matrices[7]. That report, however, speculated that myosin IIA functioned as a squeezing force, which may be a separate function for this motor.

Morphologically, the walking mode facilitated by myosin IIA used multiple contacts that may be somewhat similar to the eupodia described for the amoeba *Dictyostelium*[33]. Molecular imaging has shown that clusters of myosin IIA move inward toward the center of these contacts and that this movement is coincident with extinguishing of the contact and release from the substrate[14]. Our data are in agreement with work showing that two-dimensional motility in *Dictyostelium* relies on myosin II contractility to provide cortical tension and de-adhesion from the substrate[34]. Further evidence for the involvement of myosin IIA in the disassembly of actin and thus a potential function of myosin IIA in extinguishing cortical adhesive contacts with the substrate has been reported[35]. A millipede motility mode during migration along the inner face of HEVs[36] may also be a variant of this walking mode.

A general theme emerging from our work is a role for myosin IIA in controlling adhesion independently of substrate composition. Thus, T cells lacking myosin IIA overadhere to HEVs, other T cells and artificial substrates, whether they are coated with integrin ligands or blocked from integrin binding. This is partly consistent with reports suggesting that myosin IIA has a role in uropodal detachment from highly adhesive integrin ligand–coated two-dimensional surfaces[15,16]. This has been proposed to involve linkage of myosin IIA to LFA-1 to mediate de-attachment without affecting the regulation of LFA-1 affinity[15]. Although our results do not exclude such a possibility, we prefer the interpretation that the role of myosin IIA in adhesion may be indirect and not strictly linked to integrin adhesion. The specific effects that were confined to the uropod in the previously published studies could have been due to the specific adhesive properties of the surfaces, cells or drugs used in those different experimental systems.

In sum, our data suggest that the greater turning and lower velocity of MyoIIA-cKO T cells *in vivo* may be determined by a diminished capacity to limit contacts with their environment. We did not find evidence that the FRC network was a substrate for this greater adhesion *in vivo*. However, our results indicate that the overadhesive properties of myosin IIA–deficient T cells caused abnormal attachment to other T lymphocytes. In the lymph node, even brief spreading of the cell cortex of one T cell onto the cortex of another, particularly when cells are moving with opposite trajectories, would oppose efficient forward movement. Although it has been reported that loss of myosin IIA can affect neutrophil polarity[37] and alter T cell morphology[13], our data suggest that loss of polarity is not the main defect of T cells depleted of myosin IIA. In particular, in microchannels we did not observe excessive directional changes of cells in which myosin IIA was inhibited, and their lower response to a chemotactic gradient was probably secondary to their overadhesion.

Overall, our findings suggest that by limiting surface adhesion and providing contractile force, myosin IIA optimizes lymphocyte crawling efficiency in the many environments T cells must pass through during their trafficking. In contrast to a switch in motility rate mediated only by integrins, as predicted with haptokinetic models, we propose a switch in motility rate affected by the density (degree of confinement) of the tissue and by modulation of myosin IIA function. Such a motility switch for T cells might also occur during early activation, which leads to phosphorylation of the myosin heavy chain in response to calcium signaling[13]. This can result in the reorganization of myosin filaments[38], leading to regulation of the ability of myosin IIA to crosslink and contract the actin network. Modulation of myosin IIA activity can therefore be considered an important regulator of T cell trafficking and potentially surveillance through the modulation of cell stopping.

METHODS

Methods and any associated references are available in the online version of the paper at http://www.nature.com/natureimmunology/.

Accession codes. UCSD-Nature Signaling Gateway (http://www.signaling-gateway.org): A003748, A002871 and A001417.

Note: Supplementary information is available on the Nature Immunology website.

ACKNOWLEDGMENTS

We thank P. Beemiller for help with two-photon data analysis with Imaris and Matlab software; S. Peck for assistance in maintenance of microscopes; M. Tang (Stanford Microfabrication Center) for Silicon Masters; S. Jiang for technical assistance with cell sorting; O. Khan and M. Werner for help with mouse genotyping; M. Heuze for assistance in setting up the microchannel system; and B. Sauer (Stowers Institute for Medical Research) for the pBS479 vector. Supported by the National Institutes of Health (AI52116 to M.F.K.) and the Larry L. Hillblom Foundation (R.S.F.).

AUTHOR CONTRIBUTIONS

J.J. designed, did and analyzed all experiments and wrote the manuscript; R.S.F. provided assistance with *in vivo* experiments and participated in two-photon experiments; M.A.C. and R.S.A. generated the *Myh9*$^{flox/flox}$ mice and provided reagents; A.-M.L-D. and M.P. provided assistance in establishing the microchannel fabrication technique; C.M.S. helped with tissue sectioning and staining and with mouse genotyping; and M.F.K. coordinated the project and participated in the conception and execution of experiments and in writing the manuscript.

COMPETING FINANCIAL INTERESTS

The authors declare no competing financial interests.

Published online at http://www.nature.com/natureimmunology/.
Reprints and permissions information is available online at http://npg.nature.com/reprintsandpermissions/.

1. Dustin, M.L. Stop and go traffic to tune T cell responses. *Immunity* **21**, 305–314 (2004).
2. von Andrian, U.H. & Mempel, T.R. Homing and cellular traffic in lymph nodes. *Nat. Rev. Immunol.* **3**, 867–878 (2003).
3. Cahalan, M.D. & Parker, I. Choreography of cell motility and interaction dynamics imaged by two-photon microscopy in lymphoid organs. *Annu. Rev. Immunol.* **26**, 585–626 (2008).
4. Bajenoff, M. *et al.* Highways, byways and breadcrumbs: directing lymphocyte traffic in the lymph node. *Trends Immunol.* **28**, 346–352 (2007).
5. DiMilla, P.A., Barbee, K. & Lauffenburger, D.A. Mathematical model for the effects of adhesion and mechanics on cell migration speed. *Biophys. J.* **60**, 15–37 (1991).
6. Palecek, S.P., Loftus, J.C., Ginsberg, M.H., Lauffenburger, D.A. & Horwitz, A.F. Integrin-ligand binding properties govern cell migration speed through cell-substratum adhesiveness. *Nature* **385**, 537–540 (1997).
7. Lammermann, T. *et al.* Rapid leukocyte migration by integrin-independent flowing and squeezing. *Nature* **453**, 51–55 (2008).
8. Woolf, E. *et al.* Lymph node chemokines promote sustained T lymphocyte motility without triggering stable integrin adhesiveness in the absence of shear forces. *Nat. Immunol.* **8**, 1076–1085 (2007).
9. Friedl, P., Entschladen, F., Conrad, C., Niggemann, B. & Zanker, K.S. $CD4^+$ T lymphocytes migrating in three-dimensional collagen lattices lack focal adhesions and utilize β1 integrin-independent strategies for polarization, interaction with collagen fibers and locomotion. *Eur. J. Immunol.* **28**, 2331–2343 (1998).
10. Vicente-Manzanares, M., Ma, X., Adelstein, R.S. & Horwitz, A.R. Non-muscle myosin II takes centre stage in cell adhesion and migration. *Nat. Rev. Mol. Cell Biol.* **10**, 778–790 (2009).
11. Lammermann, T. & Sixt, M. Mechanical modes of 'amoeboid' cell migration. *Curr. Opin. Cell Biol.* **21**, 636–644 (2009).
12. Pollard, T.D. & Borisy, G.G. Cellular motility driven by assembly and disassembly of actin filaments. *Cell* **112**, 453–465 (2003).
13. Jacobelli, J., Chmura, S.A., Buxton, D.B., Davis, M.M. & Krummel, M.F. A single class II myosin modulates T cell motility and stopping, but not synapse formation. *Nat. Immunol.* **5**, 531–538 (2004).
14. Jacobelli, J., Bennett, F.C., Pandurangi, P., Tooley, A.J. & Krummel, M.F. Myosin-IIA and ICAM-1 regulate the interchange between two distinct modes of T cell migration. *J. Immunol.* **182**, 2041–2050 (2009).
15. Morin, N.A. *et al.* Nonmuscle myosin heavy chain IIA mediates integrin LFA-1 de-adhesion during T lymphocyte migration. *J. Exp. Med.* **205**, 195–205 (2008).
16. Smith, A., Bracke, M., Leitinger, B., Porter, J.C. & Hogg, N. LFA-1-induced T cell migration on ICAM-1 involves regulation of MLCK-mediated attachment and ROCK-dependent detachment. *J. Cell Sci.* **116**, 3123–3133 (2003).
17. Conti, M.A., Even-Ram, S., Liu, C., Yamada, K.M. & Adelstein, R.S. Defects in cell adhesion and the visceral endoderm following ablation of nonmuscle myosin heavy chain II-A in mice. *J. Biol. Chem.* **279**, 41263–41266 (2004).
18. Zhang, D.J. *et al.* Selective expression of the Cre recombinase in late-stage thymocytes using the distal promoter of the Lck gene. *J. Immunol.* **174**, 6725–6731 (2005).
19. Srinivas, S. *et al.* Cre reporter strains produced by targeted insertion of EYFP and ECFP into the ROSA26 locus. *BMC Dev. Biol.* **1**, 1–8 (2001).
20. Sumen, C., Mempel, T.R., Mazo, I.B. & von Andrian, U.H. Intravital microscopy: visualizing immunity in context. *Immunity* **21**, 315–329 (2004).
21. Faure-Andre, G. *et al.* Regulation of dendritic cell migration by CD74, the MHC class II-associated invariant chain. *Science* **322**, 1705–1710 (2008).
22. Straight, A.F. *et al.* Dissecting temporal and spatial control of cytokinesis with a myosin II Inhibitor. *Science* **299**, 1743–1747 (2003).
23. Andrew, N. & Insall, R.H. Chemotaxis in shallow gradients is mediated independently of PtdIns 3-kinase by biased choices between random protrusions. *Nat. Cell Biol.* **9**, 193–200 (2007).
24. Bajenoff, M. *et al.* Stromal cell networks regulate lymphocyte entry, migration, and territoriality in lymph nodes. *Immunity* **25**, 989–1001 (2006).
25. Hara, T. *et al.* A transmembrane chemokine, CXC chemokine ligand 16, expressed by lymph node fibroblastic reticular cells has the potential to regulate T cell migration and adhesion. *Int. Immunol.* **18**, 301–311 (2006).
26. Katakai, T., Hara, T., Sugai, M., Gonda, H. & Shimizu, A. Lymph node fibroblastic reticular cells construct the stromal reticulum via contact with lymphocytes. *J. Exp. Med.* **200**, 783–795 (2004).
27. Snapper, S.B. *et al.* WASP deficiency leads to global defects of directed leukocyte migration in vitro and in vivo. *J. Leukoc. Biol.* **77**, 993–998 (2005).
28. Nombela-Arrieta, C. *et al.* A central role for DOCK2 during interstitial lymphocyte motility and sphingosine-1-phosphate-mediated egress. *J. Exp. Med.* **204**, 497–510 (2007).
29. Shiow, L.R. *et al.* The actin regulator coronin 1A is mutant in a thymic egress-deficient mouse strain and in a patient with severe combined immunodeficiency. *Nat. Immunol.* **9**, 1307–1315 (2008).
30. Foger, N., Rangell, L., Danilenko, D.M. & Chan, A.C. Requirement for coronin 1 in T lymphocyte trafficking and cellular homeostasis. *Science* **313**, 839–842 (2006).
31. Renkawitz, J. *et al.* Adaptive force transmission in amoeboid cell migration. *Nat. Cell Biol.* **11**, 1438–1443 (2009).
32. Malawista, S.E. & de Boisfleury Chevance, A. Random locomotion and chemotaxis of human blood polymorphonuclear leukocytes (PMN) in the presence of EDTA: PMN in close quarters require neither leukocyte integrins nor external divalent cations. *Proc. Natl. Acad. Sci. USA* **94**, 11577–11582 (1997).
33. Fukui, Y. & Inoue, S. Amoeboid movement anchored by eupodia, new actin-rich knobby feet in Dictyostelium. *Cell Motil. Cytoskeleton* **36**, 339–354 (1997).
34. Jay, P.Y., Pham, P.A., Wong, S.A. & Elson, E.L. A mechanical function of myosin II in cell motility. *J. Cell Sci.* **108**, 387–393 (1995).
35. Wilson, C.A. *et al.* Myosin II contributes to cell-scale actin network treadmilling through network disassembly. *Nature* **465**, 373–377 (2010).
36. Shulman, Z. *et al.* Lymphocyte crawling and transendothelial migration require chemokine triggering of high-affinity LFA-1 integrin. *Immunity* **30**, 384–396 (2009).
37. Xu, J. *et al.* Divergent signals and cytoskeletal assemblies regulate self-organizing polarity in neutrophils. *Cell* **114**, 201–214 (2003).
38. Dulyaninova, N.G., Malashkevich, V.N., Almo, S.C. & Bresnick, A.R. Regulation of myosin-IIA assembly and Mts1 binding by heavy chain phosphorylation. *Biochemistry* **44**, 6867–6876 (2005).

ONLINE METHODS

Targeting vector and generation of *Myh9*$^{flox/flox}$. An XbaI–NsiI genomic fragment containing exon 3 of the *Myh9* locus plus flanking introns cloned into pBluescript was used for construction of the targeting vector. An NdeI–SphI fragment was cut from this clone, blunt-ended and subcloned into the blunt-ended HindIII site between the 5′ *lox*P site and the neomycin-resistance cassette of the vector pBS479 (a gift from B. Sauer). A NotI–NotI fragment containing the genomic sequence, *lox*P sites and neomycin-resistance cassette was then cut from pBS479, blunt-ended and reinserted into the blunt-ended targeting vector cut with NdeI–SphI. In the creation of this construct, a 208–base pair SphI fragment, at a distance of 949 base pairs 3′ of the end of exon 3, was deleted. A diphtheria toxin cassette was also present in the SalI site of pBluescript at the 3′ end of the genomic sequence. The presence of the genomic locus, neomycin-resistance cassette and diphtheria toxin cassette was confirmed by restriction enzyme mapping and sequencing of the construct. Embryonic stem cells were targeted by homologous recombination and mice were generated by conventional means. Genomic DNA from embryonic stem cell colonies and F_1 mice was screened by PstI digestion and Southern blot analysis (probe, **Supplementary Fig. 1**: *Myh9*^{wt} allele, 6.2 kilobases; *Myh9*^{flox} allele, 3.8 kilobases).

Mice. *Myh9*$^{flox/flox}$ mice were crossed with *Lck*-Cre mice[18]. Littermates or age-matched *Myh9*$^{wt/wt}$–*Lck*-Cre^{+} or *Myh9*$^{flox/flox}$–*Lck*-Cre^{-} mice were used as controls. The experimental mice were on a mixed C57BL/6J-129 background. C57BL/6J × 129S1 F_1 mice (101043; Jackson Laboratories) were used as recipient mice for adoptive transfer. Ovalbumin-specific TCR–transgenic (OT-I) mice and actin-CFP mice (Jackson Laboratories) were bred in facilities of the University of California at San Francisco in accordance with the guidelines of the Laboratory Animal Resource Center of this university. All experiments involving mice were approved by the Institutional Animal Care and Use Committee of the University of California.

Generation of actin-CFP chimeric mice. These chimeric mice were generated by an established protocol[24]. They were γ-irradiated (600 rads, twice) and were reconstituted with 5×10^6 to 10×10^6 bone marrow cells from wild-type mice. Chimeric mice were allowed to reconstitute for a minimum of 8 weeks before use as recipient mice in two-photon experiments for visualization of cells of nonhematopoietic origin in the lymph node.

Cells. Naive T cells were purified from lymph nodes and spleens with the StemSep CD8 T cell negative selection kit (Stem Cell Technologies). Activated primary CD8^{+} T cells were obtained by stimulation of lymphocytes derived from OT-I mice on plates coated with anti-CD3 (2C11) and anti-CD28 (PV-1) cells were used 4 or 5 d after stimulation. Activated T cells with deletion of myosin IIA were obtained by transduction of T cells from *Myh9*$^{flox/flox}$ mice with retrovirus encoding Cre–green fluorescent protein (GFP; to eliminate myosin IIA expression) or GFP only (as a control) at 48 h after initial activation. At 72 h after transduction, GFP^{+} T cells were sorted and used for experiments; deletion of myosin IIA in the Cre-transduced T cells was routinely verified by immunoblot analysis or flow cytometry. T cells were cultured with RPMI-1640 medium (Invitrogen) with the addition of 10% (vol/vol) FCS and L-glutamine, penicillin, streptomycin and β-mercaptoethanol (complete RPMI medium). Activated T cells were cultured in complete RPMI medium with the addition of 10 U/ml of interleukin 2.

T cell labeling and adoptive transfer. Purified control and MyoIIA-cKO T cells were labeled for 25 min with CFSE (carboxyfluorescein diacetate succinimidyl ester) or CMTMR ((5-(and-6)-(((4-chloromethyl)benzoyl) amino) tetramethylrhodamine)), were washed three times and then were used in assays. All experiments were repeated with switching of the dye labeling of control and MyoIIA-cKO T cells with equivalent results. T cells (3×10^6 to 5×10^6) were adoptively transferred by intravenous injection into the tail vein of C57BL/6J × 129S1 F_1 recipients to avoid potential rejection of transferred cells due to their mixed background.

Antibodies and reagents. Rabbit polyclonal antibody to class II myosin (BT-561; BTI) was used for immunofluorescence and immunoblot analysis. Anti-PNAd-1 (Meca-79) and anti-CD62L (Mel-13) were from BD Biosciences. Anti–integrin α_4 (PS/2) and anti-LFA-1 (M17/4) were from Bio-X-cell. Goat polyclonal anti-LYVE-1 (AF2125) was from R&D Systems. Monoclonal anti-CD4 (GK1.5) and anti-CD8 (YTS169.4) conjugated to fluorescein isothiocyanate, phycoerythrin or peridinin chlorophyll protein were from BD Biosciences. Biotin–anti-CCR7 (4B12) was from BioLegend. Unconjugated monoclonal anti-CD16/CD32 (24G.2), anti-CD4 (GK1.5), anti-CD8 (YTS169.4), anti-CD62L (Mel-13) and anti-LFA-1 (M17/4) conjugated to Alexa Fluor 647 (Invitrogen) were made by the Hybridoma Core Facility of the University of California at San Francisco. Fluorophore-conjugated secondary antibodies were from Jackson ImmunoResearch Laboratories. Mouse monoclonal anti-tubulin (T5168), aprotinin, leupeptin, phenylmethylsulfonyl fluoride, sodium fluoride, iodoacetamide and sodium orthovanadate were from Sigma. Horseradish peroxidase–conjugated protein A and the detergent-compatible protein assay kit were from Bio-Rad. CFSE and CMTMR were from Invitrogen. Blebbistatin (racemic mix) was from Calbiochem and was used at a concentration of 100 μM of the racemate. Casein (Sigma) and ICAM-1–Fc (R&D Systems) were used at a concentration of 40 nM to coat glass chamberslides and microchannels (Nalge Nunc International) for 1 h at 37 °C.

Flow cytometry. Single-cell suspensions from dissociated thymuses, lymph nodes and spleen were blocked for 10 min at 4 °C with anti-CD16/CD32 and then were stained for 25 min at 4 °C. Samples were then washed and were acquired with a FACSCalibur (BD Biosciences) and analyzed with CellQuest (BD Biosciences) or FlowJo (TreeStar).

Immunoblot analysis. This was routinely done as described[13] for quantification of knockdown of myosin IIA in T cells. Immunoblot analysis of tubulin was used as a control for normalization of myosin IIA–knockdown densitometry.

Two-photon microscopy. A custom resonant scanning two-photon instrument was used with an array of four R5929 photomultiplier tubes (Hamamatsu) operating at video rate[39]. For image acquisition, a custom four-dimensional acquisition module in VideoSavant digital video recording software (IO Industries) was used[39]. For imaging of CFSE- and CMTMR-labeled lymphocytes, samples were excited with a 5-Watt MaiTai TiSaphire laser (SpectraPhysics) tuned to a wavelength of 810 nm and fitted with a FemtoControl pulse compressor (APE). Emission wavelengths of 380–420 nm (for collagen-derived second-harmonic emission), 455–495 nm (for CFP; blue), 500–550 nm (for CFSE; green) and 567–640 nm (for CMTMR; red) were acquired. For time-lapse image acquisition, each *xy* plane spanned 288 μm × 240 μm at a resolution of 0.60 μm per pixel. Images of up to 40 *xy* planes with 3-μm *z*-spacing were acquired every 20 s for 30 min.

Purified naive control and MyoIIA-cKO CD8^{+} T cells (3×10^6 to 5×10^6 each), labeled with either 2 μM CFSE or 20 μM CMTMR, were mixed at a ratio of 1:1 and were adoptively transferred by intravenous injection into the tail vein of C57BL/6J × 129S1 F_1 recipient mice or actin-CFP chimeric mice (obtained as described above). At 18 or 42 h after T cell transfer, recipient mice were killed and popliteal, inguinal and axillary lymph nodes were surgically removed and immobilized on coverslips with the medullary side adhering to the coverslip. Lymph nodes were maintained at a temperature of 35.5–37 °C in a flow chamber perfused with RPMI medium without phenol red (Gibco), saturated with a gas mixture of 95% O_2 and 5% CO_2.

Imaris software (Bitplane) was used for analysis of the three-dimensional data and for tracking of cells. Imaris and Matlab software (Mathworks) were then used to obtain T cell speed, turning angle and mean square displacement. Instantaneous velocity and turning angle distribution were calculated between two (velocity) and three (turning angle) consecutive time points for each time point of each cell in a stage position. The average median velocity and turning angle were calculated on a per-cell basis and the average of all cell values was then calculated. The mean square displacement over 10 min was calculated for each cell in a stage position and the average for each stage position was then determined; finally, the average of all stage positions from three independent experiments was calculated. The motility coefficient for each cell population in a stage position was determined by calculation of the slope of the mean square displacement curve and application of the following formula: motility coefficient = $x^2 / 6t$, where x is the slope of the MSD curve and 't' is time.

doi:10.1038/ni.1936

Transwell migration assay. Purified naive $CD8^+$ T cells from control and MyoIIA-cKO mice were labeled with 1 μM CFSE or 10 μM CMTMR, were mixed at a ratio of 1:1 and were used for Transwell migration assays. Labeled T cells (1×10^6) resuspended in RPMI medium supplemented with 1% (wt/vol) fatty acid–free BSA (Calbiochem) and 10 mM HEPES, (stock pH, 7.2–7.5) were added to the top chamber of each Transwell plate (Corning), and cells were allowed to migrate for 1 h at 37 °C in the presence or absence of chemokine. Migrated T cells were then collected from the bottom well and were quantified for a fixed period of time (2–3 min) on a FACSCalibur (BD Biosciences). A known amount of cells, acquired for the same amount of time, was used as a standard for determining the number of migrated cells.

Lymph node staining. At 2 and 48 h after adoptive transfer of control and MyoIIA-cKO naive T cells labeled with 1 μM CFSE or 10 μM CMTMR, popliteal lymph nodes of recipient mice were collected and snap-frozen in optimum cutting temperature compound (Tissue-Tek). Lymph node sections 10 μm in thickness were fixed with 1% (vol/vol) paraformaldehyde, then were blocked and stained. Anti-PNAd-1 was used for visualization of HEVs, and anti-LYVE-1 was used to highlight lymphatic sinuses. Images of whole lymph node sections were acquired on a confocal microscope with the scan-slide function of Metamorph (Universal Imaging). Data were then analyzed with Imaris software for the identification of T cells on the basis of their CFSE or CMTMR fluorescence, followed by the creation of a surface mask of the stained HEVs or lymphatic sinuses. The frequency of T cells in contact with HEV surfaces or lymphatic sinuses was then quantified with the 'spot–to–surface distance' function of Imaris. Multiple lymph node sections were analyzed with an average of 50 cells per group per lymph node section. An average of four lymph node sections per experiment was analyzed.

T cell lymph node homing and egress. Control and MyoIIA-cKO T cells were labeled with 1 μM CFSE or 10 μM CMTMR and mixed at a ratio of 1:1, and 2×10^6 to 4×10^6 T cells were injected intravenously into recipient mice. At 2, 18 or 42 h after adoptive transfer, lymph nodes, blood and spleens were collected from the recipient mice. After dissociation of lymph nodes and spleens, the frequency of transferred control and MyoIIA-cKO T cells was quantified by flow cytometry and the ratio of MyoIIA-cKO to control T cells in the blood, inguinal lymph nodes and spleen of recipient mice was determined. The ratios in lymph node and spleen were normalized to the ratio in blood to correct for potential differences in the input or survival of control and MyoIIA-cKO cells.

For analysis of the egress rate and lymph node retention of control and MyoIIA-cKO T cells, transferred T cells were allowed to equilibrate for 24 h in recipient mice and then the mice were treated with PBS or entry-blocking antibodies. Anti-CD62L or a combination of anti-LFA-1 and anti–integrin α_4 was used with similar results. At 18 h after the treatment with blocking antibody, the ratio of MyoIIA-cKO T cells to control T cells retained in the inguinal lymph nodes of recipient mice was assessed as described above.

Adhesion to ICAM-1 under flow. Naive control and MyoIIA-cKO $CD8^+$ T cells were labeled with 1 μM CFSE or 10 μM CMTMR, mixed at a ratio of 1:1 and injected into flow chambers (IBIDI) for 2 min at a shear flow of 0.25 dyne/cm^2, then were subjected to 10 min of physiological shear flow (2 dyne/cm^2). Brightfield and fluorescent images were then acquired and adherent cells at the end time point were quantified with Metamorph software.

Microchannel fabrication and imaging. Microchannel fluidic devices were fabricated by a soft lithography technique with PDMS (polydimethylsiloxane; Sylgard Elastomer 184 kit; Dow Corning) as described[21]. PDMS was poured onto the stamp and left to cure overnight under vacuum; once solidified, the PDMS with embedded microchannels was then cut from the mold and an entry port was cut adjacent to the channel structures. The PDMS and a glass-bottomed imaging dish (Fluoro Dish, World Precision) were then activated for 30 s in a plasma cleaner (Harrick Plasma) and bonded to each other. After 1 h of incubation at 55 °C, microchannel imaging chambers were then put back in the plasma cleaner and left under vacuum for 5 min, after which the plasma source was activated for 15 s. Immediately after that step, 10 μl fibronectin solution (50 μg/ml), ICAM-1 solution (5 μg/ml) or casein solution (20 μg/ml) was injected into the entry area of the microchannels to coat them. After 1 h of incubation at 37 °C, excess coating proteins were washed out with PBS and imaging media was added. T cells (1×10^5 to 3×10^5 cells resuspended in 10 μl) were then added to the entry port and were allowed to spontaneously enter the channels at 37 °C for 2–4 h (for activated T cells) or overnight (for naive T cells). T cells crawling in the microchannels were then imaged for 1–6 h at intervals of 30 s or 90 s with a 20× phase-contrast objective or a 20x brightfield objective. T cells remained alive and motile for the entire period of recording. Metamorph software (Molecular Devices) was used for calculation of cell speed, adhesion time and weave cycle. Typically a minimum of ten cells per microchannel width per treatment condition were analyzed.

TIRF microscopy. A modified Axiovert 200M microscope fitted with a Zeiss TIRF slider and a 100× oil-immersion objective with a numerical aperture of 1.45 was used for TIRF imaging. TIRF images were acquired with a liquid-cooled intensified charge-coupled device camera (model XR/Mega-10Z; Stanford Photonics). The TIRF microscope was equipped with 491-nm (50-mW) and 561-nm (25-mW) solid-state lasers (Cobolt) and excitation wavelength was selected through an acousto-optic tunable filter (Neos). Emission wavelengths were selected through the combination of a multiple-edged dichroic and multiple-pass emission filter. The control and imaging software was InVivo (QED Imaging; Media Cybernetics). The microscope was configured with a heated stage to maintain a sample temperature of 37 °C.

For TIRF imaging of surface adhesion zones, activated T cells were labeled with 4 μM CMTMR. T cells (5×10^4) were plated overnight in glass chamber slides or alternatively T cells (1×10^6) were injected into microchannels of various sizes. For time-lapse experiments, brightfield and TIRF fluorescence images were acquired every 5 s for 5 min. For the prevention of photoinactivation, crosslinking and toxicity of blebbistatin, which may occur after illumination with light of a wavelength less than 500 nm (ref. 40), TIRF imaging of blebbistatin-treated cells was done with CMTMR labeling and illumination of the cells with a 561-nm laser.

Contact areas were measured with Metamorph software, a threshold was set for the CMTMR fluorescence in the TIRF channel and the area of the fluorescent region was then calculated with the region statistics function of Metamorph. The crawling mode was assessed as described[14]: if the CMTMR TIRF fluorescence during the time lapse showed only one main adhesion area, the cell was considered to be sliding; if multiple distinct adhesion zones were present, the cell was considered to be walking. The crawling mode of cell with multiple adhesion zones was considered to be mixed if it consecutively presented a single adhesion zone for more than half the duration of a time lapse. The shape factor, which indicates how closely a cell resembles a circle, was calculated as follows: $(4 \times \pi \times \text{area}) / \text{perimeter}^2$, with values close to 0 indicating an elongated cell and a value of 1 representing a perfect circle. T cell ellipticity was calculated as follows: cell length (span of the longest cord through the cell) / cell breadth (width of the cell perpendicular to the longest cord). These morphology parameters were calculated with Metamorph with the brightfield images acquired during TIRF imaging.

Stromal cell lines. Primary cell lines of lymphoid stroma were obtained by complete digestion of C57BL/6J lymph nodes with collagenase A and collagenase D according to a published protocol[26]. After complete digestion, the final cell pellet was sorted for FRCs ($CD45^-CD35^-CD31^-gp38^+$) or lymphatic endothelial cells ($CD45^-CD35^-CD31^+gp38^+$).

T cell coupling assay. Naive control and MyoIIA-cKO $CD8^+$ T cells were labeled with 1 μM CFSE and coupled to FRCs, lymphatic endothelial cells, DCs or wild-type T cells labeled with 10 μM CMTMR. For coupling, cells were spun together for 1 min at 200*g* and were incubated for 10 min at 37 °C, then were gently resuspended and then fixed with 1% (vol/vol) paraformaldehyde. Cells were then washed and the frequency of conjugate formation was quantified by flow cytometry.

Statistical analysis. Prism software (GraphPad) was used for graphing the data and for calculation of statistical significance by Student's *t*-test for single comparisons or analysis of variance for multiple comparisons, followed by post-hoc Tukey tests on continuous variable data, which was normally distributed and had equal variance. Alternatively, Kruskal-Wallis or Mann-Whitney tests were

used for non–normally distributed data for determination of statistical significance, followed by Dunn post-tests for calculation of *P* values for multiple comparisons. The chi-squared test was used for calculation of the significance of nominal variable data.

39. Bullen, A., Friedman, R.S. & Krummel, M.F. Two-photon imaging of the immune system: a custom technology platform for high-speed, multicolor tissue imaging of immune responses. *Curr. Top. Microbiol. Immunol.* **334**, 1–29 (2009).
40. Kolega, J. Phototoxicity and photoinactivation of blebbistatin in UV and visible light. *Biochem. Biophys. Res. Commun.* **320**, 1020–1025 (2004).

doi:10.1038/ni.1936